metals

MDPI

Article

Functional Behaviour of Cold-Worked and Straight-Annealed NiTi Elements Processed with Ultrashort Laser Cutting

Carlo Alberto Biffi * and Ausonio Tuissi

National Research Council, Institute of Condensed Matter Chemistry and Technologies for Energy, Via G. Previati 1E, 23900 Lecco, Italy

* Correspondence: carloalberto.biffi@cnr.it

Abstract: Among functional materials, quasiequiatomic NiTi alloys are one of the most promising and diffused for some sectors, from the biomedical to aerospace ones. Their peculiar performance, namely, shape memory effect and pseudoelasticity, is induced via a thermomechanical treatment called shape setting or with the heat treatment of annealing. This heat treatment is carried out in cold-worked conditions. The present work studies the effect of the material conditions of straight annealing and cold working on the functional performance of diamond-shaped NiTi microdevices realised through ultrashort laser cutting. In detail, experiments were carried out aimed at studying the effect of laser power, scanning speed, and number of passes on the kerf width with the focus on defining the most suitable process condition on both straight-annealed and cold-worked sheets of 100 µm in thickness. After the process parameters had been defined, the transformation temperatures and superelastic behaviour were analysed though differential scanning calorimetry and force–displacement testing. The femtosecond cutting of straight-annealed NiTi did not change the characteristic temperatures of the base material, while the same process induced a soft martensitic transformation with respect to the cold-worked material due to a heat accumulation effect.

Keywords: NiTi alloy; shape memory alloys; laser cutting; ultrashort laser cutting; superelasticity

Citation: Biffi, C.A.; Tuissi, A. Functional Behaviour of Cold-Worked and Straight-Annealed NiTi Elements Processed with Ultrashort Laser Cutting. *Metals* **2023**, *13*, 16. https://doi.org/10.3390/met13010016

Academic Editor: Yiping Tang

Received: 11 November 2022
Revised: 12 December 2022
Accepted: 15 December 2022
Published: 22 December 2022

1. Introduction

Among shape memory alloys (SMAs), intermetallic NiTi is the most diffused for different sectors of applications, from biomedicine to aerospace, including its use in actuators, sensors, and dampers [1–4].

In the industrial environment, laser cutting is largely adopted for manufacturing stents and catheters in NiTi, and for sensor and actuation devices [5].

The use of the laser beam can alter the NiTi microstructure due to the heat transfer within the material [6], but also the Ni/Ti ratio, which can alter the final performance [7]. In fact, the use of long [6] or short [8–10] laser pulses promotes relevant heat transfer into the material; therefore, some thermal damage such as microstructural changes, cracks, oxidation, and the modification of the chemical composition are typical defects altering the initial shape memory effect or the superelasticity of the NiTi material. The main reason for these thermal defects is related to the creation of the liquid pool that can induce the heat conduction of the thermal wave into the material. These effects can be limited by using ultrashort laser pulses that can induce the sudden vaporisation of the material with a limited contribution of fusion for giant laser peak powers [11–13]. Several works in the literature show that the ultrashort laser processing of NiTi SMAs can offer a high level of precision and negligible microstructural alteration [14–18]. Additionally, other technological solutions for limiting the heat transfer are the performance of laser cutting under a liquid [19], using water-jet-guided laser-beam machining [20], and short-emission wavelengths in the green and ultraviolet fields [15,21]. Good functional performance can be achieved, but their use in the industrial environment is far from real application.

In all these solutions, the correlation between the temperature and time of the imposed thermal cycle are not the only parameters that can affect the final functional properties of NiTi elements. The initial microstructure can be another relevant aspect that can limit or amplify the effect of the heat transfer on the microstructural evolution and the corresponding functional behaviour of NiTi SMAs [22,23].

Moreover, other difficulties can be found in the laser cutting of NiTi in cold-worked condition, which exhibits a finer microstructure, and the risk of sensibility to the heat is higher [24].

For this reason, the present study has the goal of investigating the effect of the initial microstructure of a Ni-rich NiTi alloy considered in cold-worked and straight-annealed conditions on the laser-cutting performance and the corresponding functional performance of diamond-like elements.

2. Experimental

2.1. Laser-Cutting Process

Straight-annealed and cold-worked 100 µm thick superelastic NiTinol sheets (etched condition, supplied by the Memry-Saes Group) were laser-cut using a femtosecond laser source (mod. Pharos-10W from Light Conversion). The main characteristics of the laser source used for cutting are listed in Table 1.

Table 1. Technical specifications of the femtosecond laser source used for the cutting experiments.

Characteristics	Value
Max average power	10 W
Pulse duration	<290 fs
Pulse duration range	290 fs–20 ps
Max pulse energy	>0.2 mJ
Beam quality	TEM00; $M^2 < 1.2$
Base repetition rate	1 kHz–1 MHz
Central wavelength	1028 ± 5 nm
Waist diameter	30 µm

Process optimisation was first performed on the straight-annealed (SA) NiTi sheets, varying the number of laser passes (N = 50, 120, and 200), average power (P = 5, 7.5, and 10 W), and scanning speed (v = 300, 550, and 800 mm/s) in a full factorial design. Three linear cuts, 15 mm in length, were replicated for each process condition. The fixed process parameters were the following: (i) repetition rate = 600 kHz; (ii) focus position, placed on the top surface; (iii) no assist gas.

In the case of the cold-worked (CW) sheet, only the number of the laser passes (N = 50, 100, 125, 150, and 175) was investigated. The cutting experiments were carried out in the condition with the following process parameters: (i) P = 10 W; (ii) v = 550 mm/s.

These choices were made for the following reasons: the cold-worked material was internally prepared because it is not achievable in the market; therefore, its amount was limited. Moreover, due to the large strain hardening introduced in the material, the base NiTinol sheets were irregular. This aspect introduced some focus shift during the cutting; therefore, we investigated the effect of the number of laser passes, starting from the combination of laser power and scanning speed (indicating the energy required for laser processing the NiTi alloy) selected from the straight-annealed material.

After the selection of the most suitable process condition for straight-annealed and cold-worked NiTi, the diamond-like elements were laser-cut in both material conditions, as depicted in Figure 1.

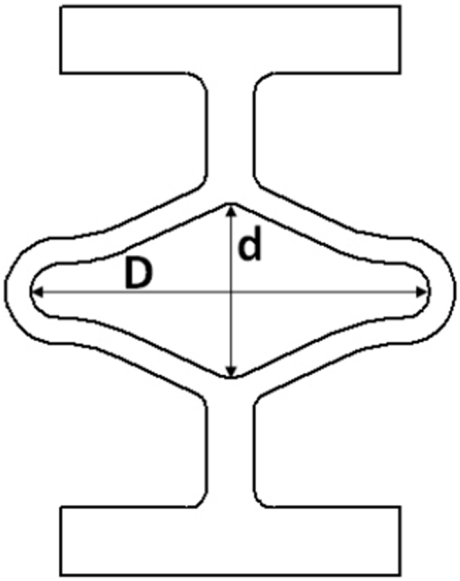

Figure 1. Schematic of the laser-cut diamond-shaped device (D = 5.9 mm and d = 1.7 mm).

2.2. Chemical Etching

After laser cutting, the diamond elements were also subjected to chemical etching in order to remove the dross and surface irregularities caused by the thermal processing. The acid solution used for this process comprised 50% H_2O, 40% HNO_3, and 10% HF for 2 min. This procedure was applied for the elements subjected to stress–strain testing.

2.3. Characterisations

The samples containing the linear cuts and the diamond-like elements were analysed with a scanning electron microscope (Leo Electron Microscope 1430, Zeiss, Aalen, Germany).

Mechanical testing was carried out with dynamic mechanical analysis (DMA, mod. Q800 from TA Instruments, United States) to obtain the force–displacement response at different temperatures (30 and 100 °C). The maximal applied force was 17.9 N with a loading/unloading rate of 0.200 N/min.

The operating temperatures of the martensitic transformation were detected with a differential scanning calorimeter (DSC, mod. SSC 5200 from Seiko Instruments, Japan). Complete thermal cycles were carried out within a temperature range between −100 and +100 °C, with a heating/cooling rate of 10 °C/min.

3. Analysis of Results

3.1. Femtosecond Laser Cutting of Straight-Annealed NiTi Sheets

The process–ability map obtained from the full factorial analysis performed at varying laser power levels, scanning speeds, and number of laser passes on NiTi straight-annealed sheets is reported in Table 2.

In the case of 50 scans, only one condition was able to realise a through cut of the sheet. This was the case of the cut with the highest power and the lowest process speed, producing the maximal energy transferred to the material. By increasing the number of scans to 120 and 200, the process–ability window could produce an enlarged through cut and lower power values. Even with the adoption of 200 scans, the lowest studied power of 5 W was not able to generate through cuts with any studied process speed level because the energy was too low.

Table 2. Process–ability map indicating the realisation of complete through-cut edges (represented by X) and blind-cutting edges (represented by O) while varying the investigated process parameters.

Number of Laser Passes	**Speed (mm/s)**		
***n* = 50**			
Power (W)	**800**	**550**	**300**
10	X	X	O
7.5	X	X	X
5	X	X	X
***n* = 120**	**Speed (mm/s)**		
Power (W)	**800**	**550**	**300**
10	X	O	O
7.5	X	X	O
5	X	X	X
***n* = 200**	**Speed (mm/s)**		
Power (W)	**800**	**550**	**300**
10	O	O	O
7.5	O	O	O
5	X	X	X

The through cuts were evaluated with SEM analysis. The most representative SEM pictures of the laser-cutting edges are shown in Figure 2, while the measurements of the entry and exit kerf widths, performed only in the case of complete through cuts, are depicted in Figure 3. The SEM images allowed for carrying out qualitative analysis for evaluating the integrity of the kerf, such as the uniformity of the kerf width and the presence of recast material. In particular, the amount of recast material in the selected process conditions of Figure 2 varied largely. In the case shown in Figure 2a,b, the recast material was quite limited and it was present almost only in the exit side, while it increased largely in the case of Figure 2c, placed on both the entrance and exit sides. A higher amount of recast can depend on the excess of energy supplied to the material.

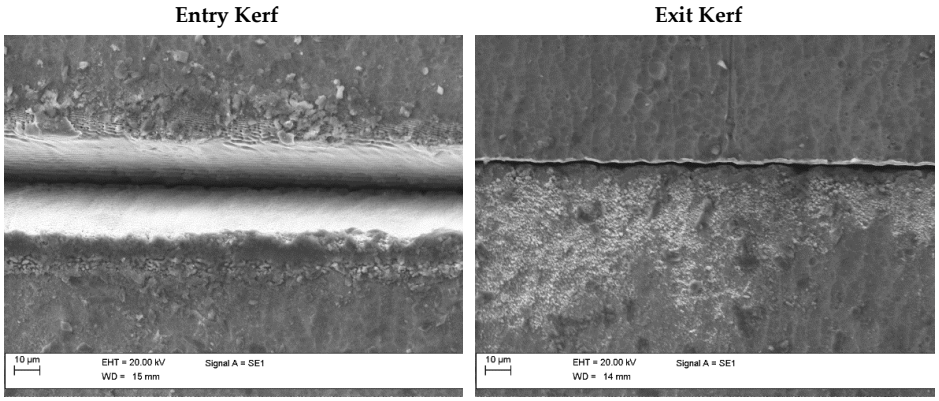

(**a**)

Figure 2. *Cont.*

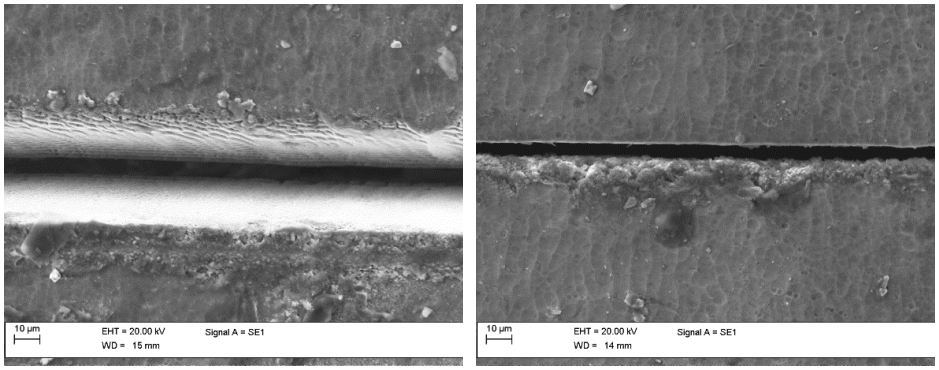

(**b**)

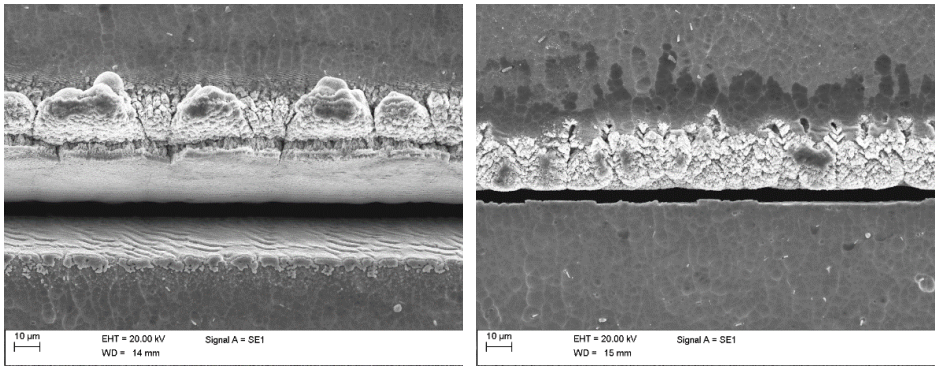

(**c**)

Figure 2. SEM images of the entry and exit kerfs produced with different process conditions: (**a**) P = 10 W; v = 550 mm/s; *n* = 120; (**b**) P = 10 W; v = 300 mm/s; *n* = 120; (**c**) P = 10 W; v = 300 mm/s; *n* = 200.

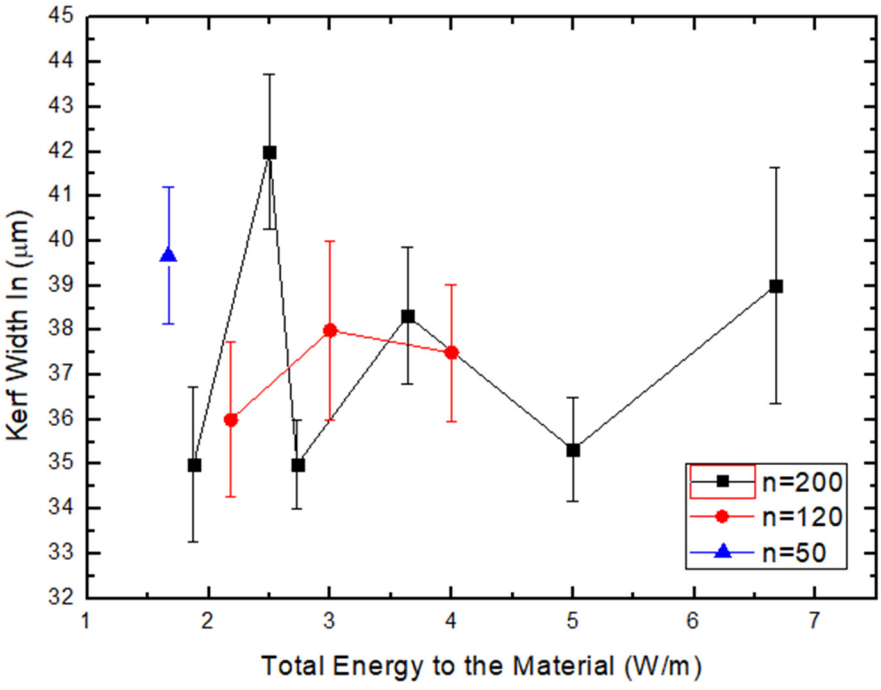

(**a**)

Figure 3. *Cont.*

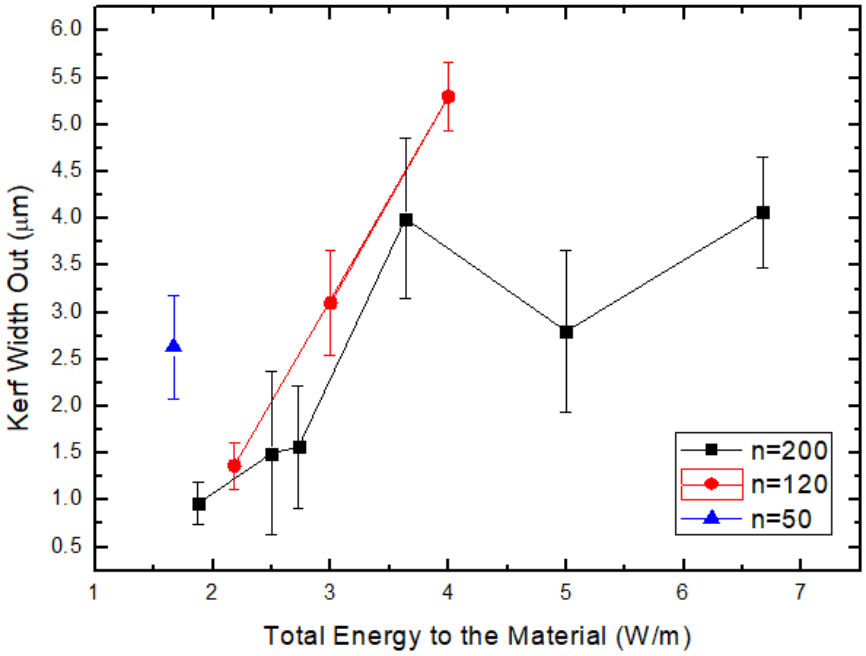

(**b**)

Figure 3. Kerf width on the (**a**) entry and (**b**) exit sides of the cut versus the total energy supplied to the material.

Figure 3 shows the kerf widths on the entry and exit sides of the cuts, only in full penetration conditions. The analysis was carried out in relation to the kerf width with the total energy E given the material, which could be calculated as shown in Equation (1):

$$E = \frac{P}{v} * n \quad (1)$$

where P is the laser power, v the scanning velocity, and n the number of scans.

Figure 3 shows that the trends for the entry and the exit sides were completely different. On the entry side, the kerf width was almost distributed in an interval in the range of around 33–44 μm. The variability in the measurements was not dependent on the specific process condition, and it mainly depend on the laser beam size that was incident on the upper surface.

On the other hand, the exit kerf showed different behaviour. It tended to increase when the total energy increased for the number of laser passes equal to 120 and 200. As it could be expected, higher energy increased the material removal rate and consequently increased the width of the exit kerf. The same trends could be observed on a smaller scale among the cuts performed with the same number of scans. The dross was the main feature that generated irregularities on the exit surface and created the variability in the observed kerf.

In order to define the best condition for the cut, both geometrical and heat accumulation considerations needed to be taken into account. The use of the highest number of laser passes promoted a large amount of recasting because of the exceeding energy; therefore, these conditions cannot be considered to be suitable for the precise cutting of NiTi functional elements. With the use of 120 number of laser passes, the condition characterised by P = 10 W and v = 550 mm/s allowed for achieving a reasonable fine kerf width, and limited oxidation and heat alteration.

Under this selected process condition, it was possible to cut through the straight-annealed sheet, generating minimal effects on the base material, which preserved its functionality.

3.2. Laser Cutting of Cold-Worked NiTi Tapes

The cold-worked NiTi alloy presented higher sensitivity to heat, hindering the process for the two following reasons: (i) from a microstructural point of view, its microstructure was finer than that of the straight-annealed alloy, so a smaller amount of heat could thermally damage the material much more; (ii) from a technological point of view, the high degree of plastic deformation required to suppress the martensitic transformation rendered the sheets less flat, so the laser cutting appeared to be more unstable. Some possible issues, such as possibly being out of focus, variable focal distance, and the motion of the part during the cutting for material relaxation, could render the laser-cutting process less repeatable and more unstable in the realisation of a complete through-cut edge.

First, a study to understand how to realise a through cut on a cold-worked sheet was carried out, keeping all the parameters obtained for the straight-annealed sheet optimisation constant, and only varying the number of scans during the process due to the two following reasons: (i) cold-worked and straight-annealed sheets have the same chemical composition, so the energy required by the material to be vaporised and partially melted can be assumed to be constant; (ii) due to the deflections of the cold-worked sheets, it was assumed that the number of laser pulses could be adjusted to achieve a through and stable cutting.

The experiments were carried out at varying number of scans of 50, 100, 125, 150, and 175. Figure 4 shows the SEM images of the cutting edges at both the entrance and exit sides, carried out in some representative process conditions. The use of 50 laser scans allowed for achieving a blind kerf, as the total energy transferred to the material was below the threshold: this result was in good agreement with the previous results obtained for straight-annealed NiTi tapes. Therefore, SEM analysis was carried out only for the through cutting edges. The morphology of the kerf appeared to be more irregular in the case of the cold-worked alloy, and the dross formation was more intense than that in the case of the straight-annealed alloy. As previously mentioned, cold-worked tapes are characterised by a finer microstructure, induced by cold rolling, and by consequent residual stresses. The latter feature can be released by the thermal energy coming from the laser beam in the form of the distortion of the NiTi tapes, provoking an unstable condition of cutting not entirely inside the depth of field. The presence of a higher amount of dross could have been due to the more difficult material evacuation during the cutting.

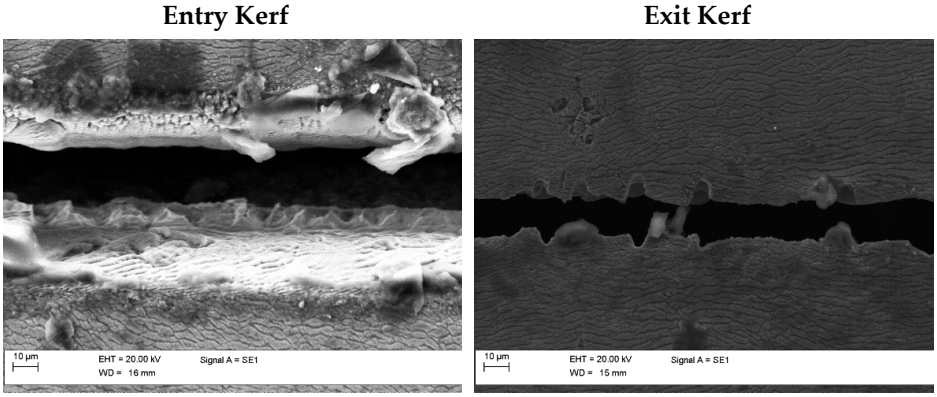

(**a**)

Figure 4. *Cont.*

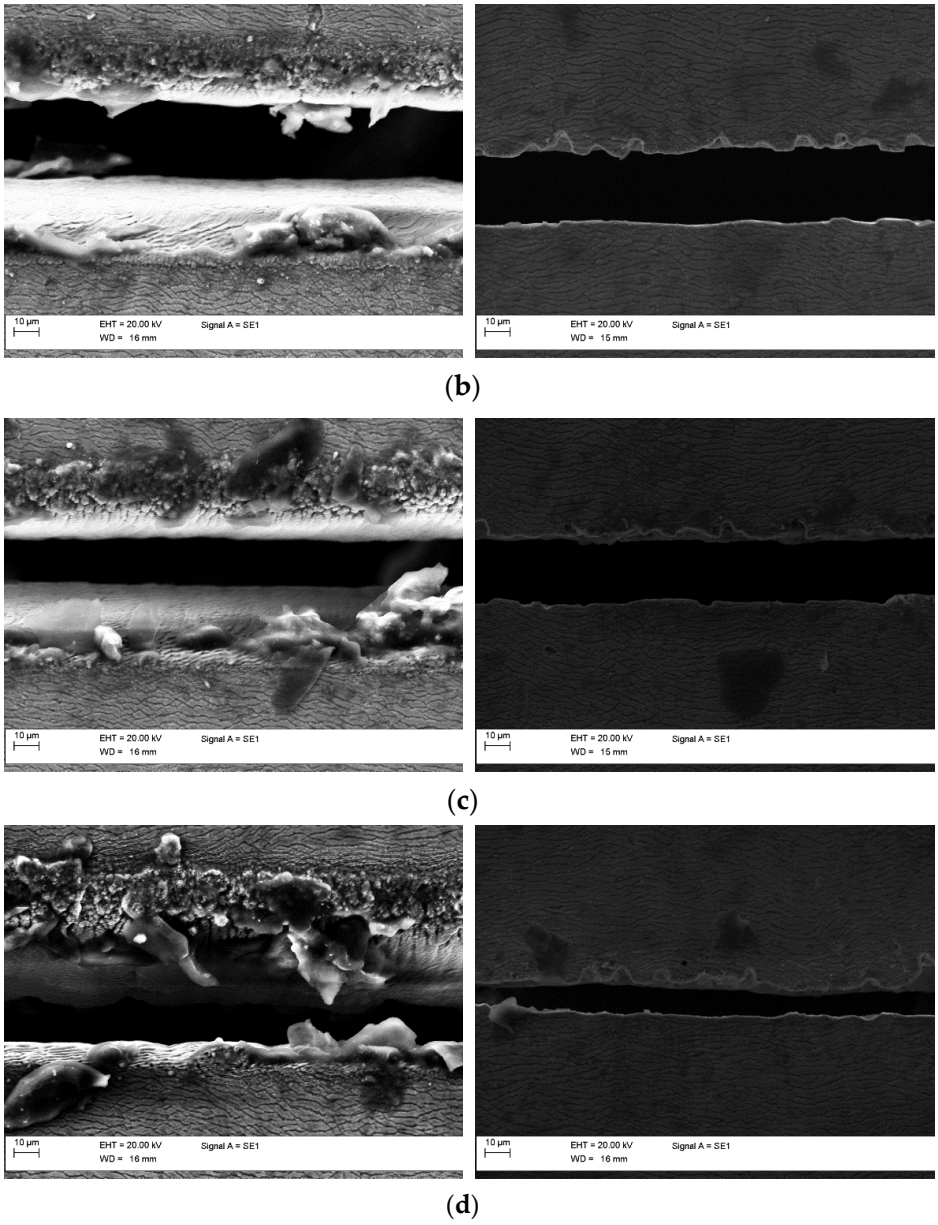

Figure 4. SEM images of the entry and exit kerfs at varying numbers of laser passes on the cold-worked NiTi sheet: (**a**) P = 10 W; v = 550 mm/s; *n* = 100; P = 10 W; (**b**) v = 550 mm/s; *n* = 125; (**c**) P = 10 W; v = 550 mm/s; *n* = 150; (**d**) P = 10 W; v = 550 mm/s; *n* = 175.

By increasing the number of laser scans, the damage caused to the material became more evident, shown by the presence of a larger amount of recast material on the cutting edge.

Figure 5 shows the evolution of the kerf width values measured at the entrance and exit sides. The graph shows that a parabolic trend of both kerf widths was achieved with the increase in the number of laser passes. In detail, at 50 scans, the width on the entry kerf was below 10 µm, while for a higher number of laser passes (from 100 up to 150 scans), the width was in the range of 20–30 µm; for 175 scans, it was reduced down to 15 µm.

The limited dimension of the kerf realised at 50 laser passes depended on the insufficient energy transferred to the material; therefore, the cutting edge did not completely penetrate the tape thickness. By increasing the number of laser passes, the total energy was increased sufficiently for promoting a complete through cutting edge.

After this investigation, the best conditions for cutting the cold-worked NiTi tapes were the following: P = 10 W; v = 550 mm/s; *n* = 150 scans.

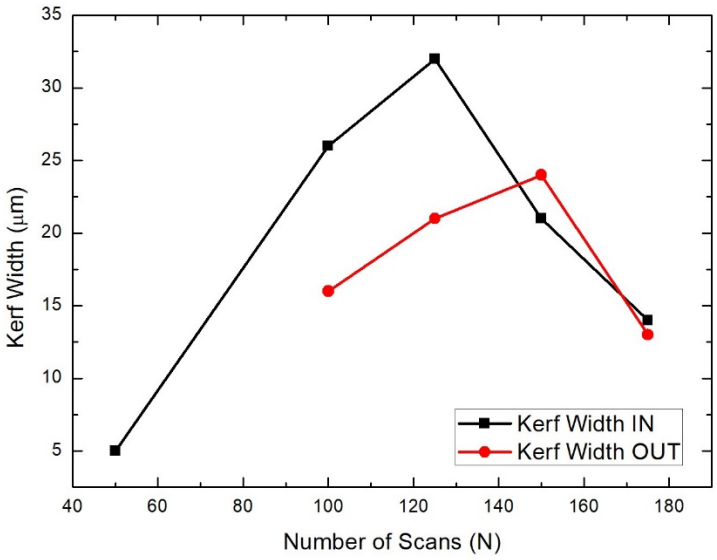

Figure 5. Trend for entry and exit kerfs of linear cuts on cold-worked NiTinol sheet at varying numbers of laser passes.

3.3. Processing of Straight-Annealed and Cold-Worked Diamond-like Elements

According to the process parameter selection carried out in the previous sections of this work, diamond-like elements in SA and CW NiTi were laser-cut. A representative images of an NiTi element is shown in Figure 6. Some samples were left in the as-cut condition, while others were subjected to chemical etching for removing the residuals of the drops of melted material, which could be found on the element border. The procedure indicated in the experiment section was implemented in the same way for both the SA and CW NiTi elements. SEM images showing the curvature of the diamond-like element as representative of the most critical part of the NiTi element in the as-cut and chemical etched conditions are shown in Figure 7. The present analysis was carried out to check the quality of the final surface of the NiTi elements. After chemical etching, the borders were cleaner from some small irregularities, linked to some residuals from the limited melting and the vaporisation of the alloy.

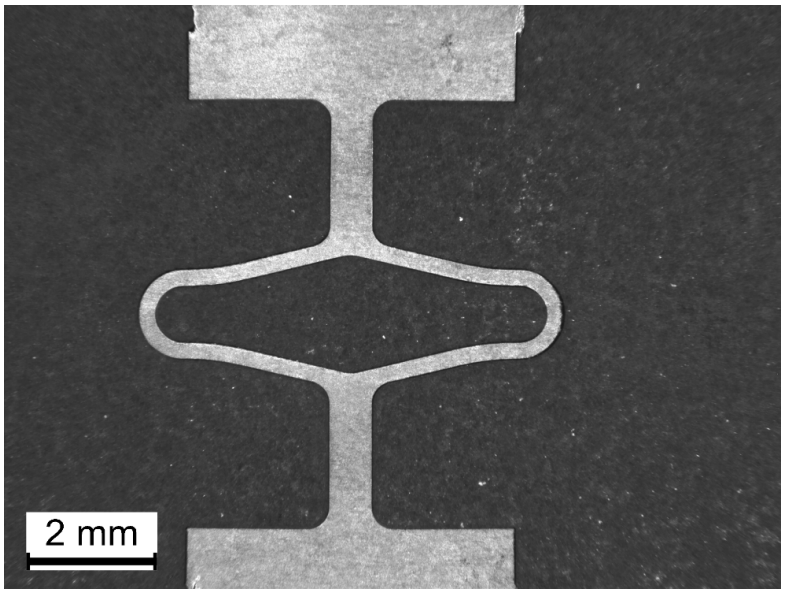

Figure 6. Representative image of a diamond-like element, laser-cut from the straight-annealed NiTi sheets.

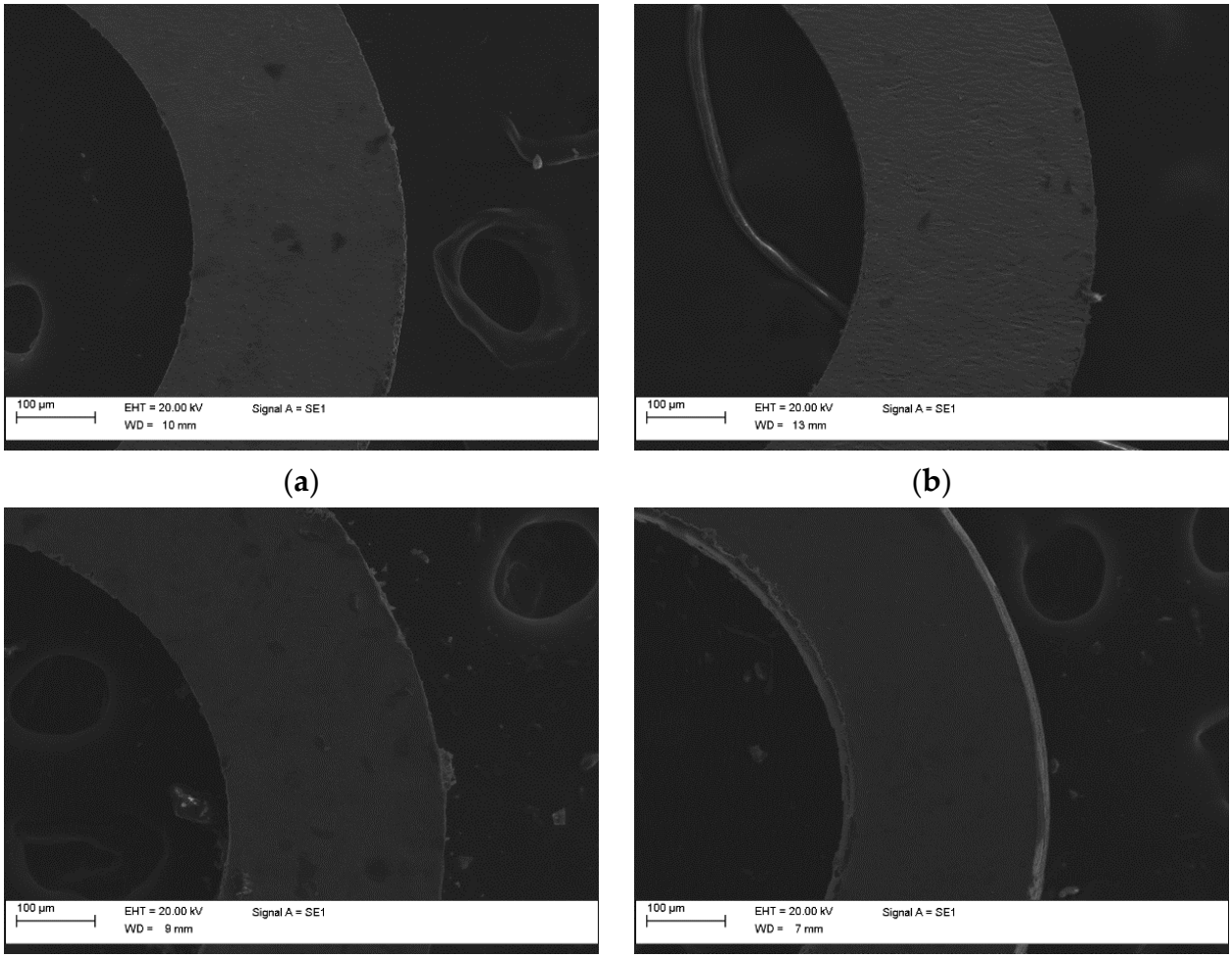

Figure 7. SEM images of a representative portion of the diamond-like element, laser-cut from straight-annealed sheet (**a**) before and (**b**) after chemical etching, and from cold-worked sheet (**c**) before and (**d**) after chemical etching.

3.4. Functional Characterisation of Straight-Annealed and Cold-Worked Diamond-like Elements

The functional characterisation of the NiTi diamond-like elements in both the SA and CW conditions was carried out through differential scanning calorimetry in order to detect the transformation temperature and through-force–displacement curves, obtained upon loading and unloading, to test the superelasticity.

In detail, the DSC scans of the laser-cut sample were analysed and compared with the ones of the initial material present in the SA condition (see Figure 8). The two DSC scans almost completely overlapped with each other. The peaks of the martensitic transformation (MT) of the SA laser-cut diamond-like element were slightly shifted towards lower temperatures, probably due to the limited heating correlated to the laser-cutting process. This result was in good agreement with the ultrashort laser cutting of NiTi SMAs already published in the literature [6]. In fact, vaporisation induced by ultrashort laser cutting can largely limit the heat transfer in the material of the workpiece, provoking a negligible thermal alteration.

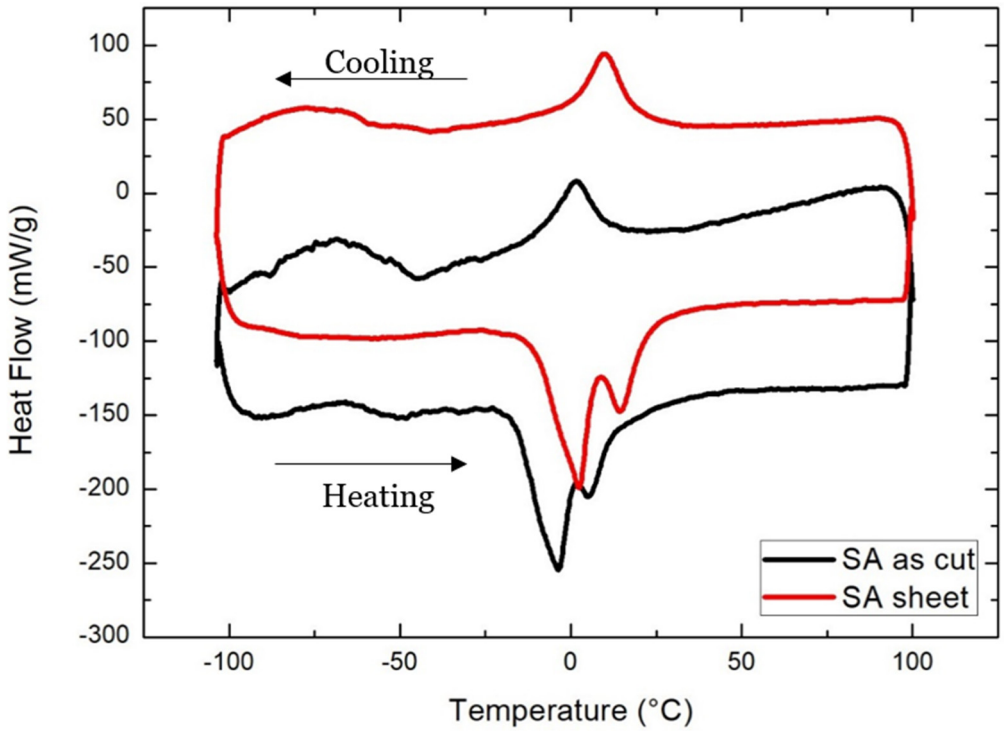

Figure 8. DSC scans of the straight-annealed sheet and the laser-cut diamond-like element.

The evolution of the superelasticity of the diamond-like element, laser-cut in SA condition, was studied via the static force/displacement curves, performed at low (30 °C) and high (100 °C) temperatures, and is reported in Figure 9. In good agreement with the DSC characterisation, the element was fully austenitic at 30 °C. In fact, the typical flaglike curve was revealed during the loading/unloading testing. A force of 1.6 N was achieved at the plateau of the force/displacement curve upon loading, and about 0.7 N upon unloading.

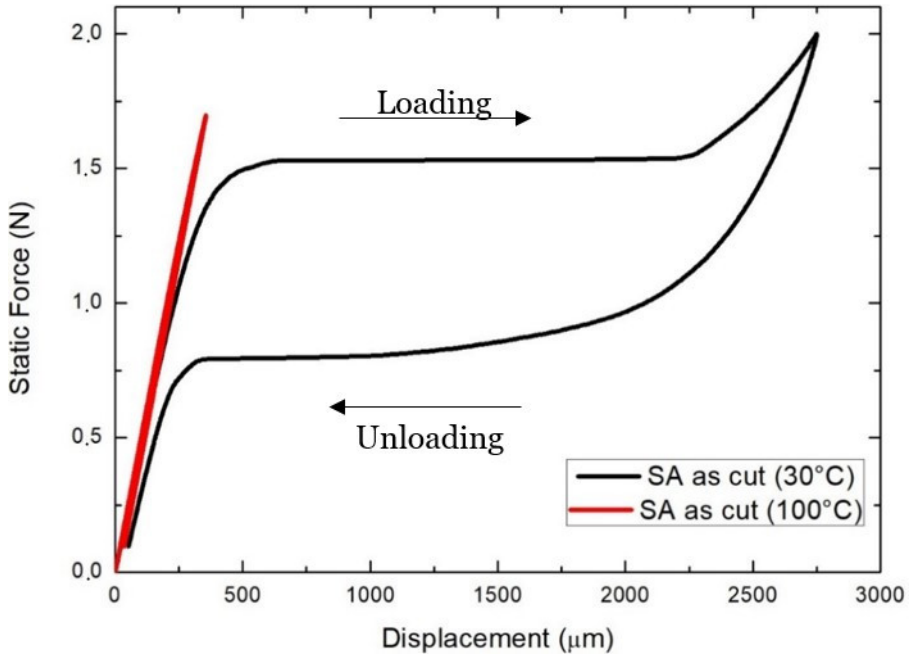

Figure 9. Static force/displacement curve of SA diamond-like element at low (30 °C) and high (100 °C) temperatures.

On the other hand, when heated up to 100 °C, the element lost the superelastic behaviour, and only a linear path upon loading and unloading was reached. Figure 10 shows the superelastic behaviour of the SA diamond-like element in the as-cut and chemical etched conditions. The plateau force values were shifted down to lower values because of the material removal induced by the chemical etching; a similar change was also seen for the maximal displacement, which could be increased in correspondence of the etched sample. The force–displacement curves were very similar to each other, and no evident differences could be detected.

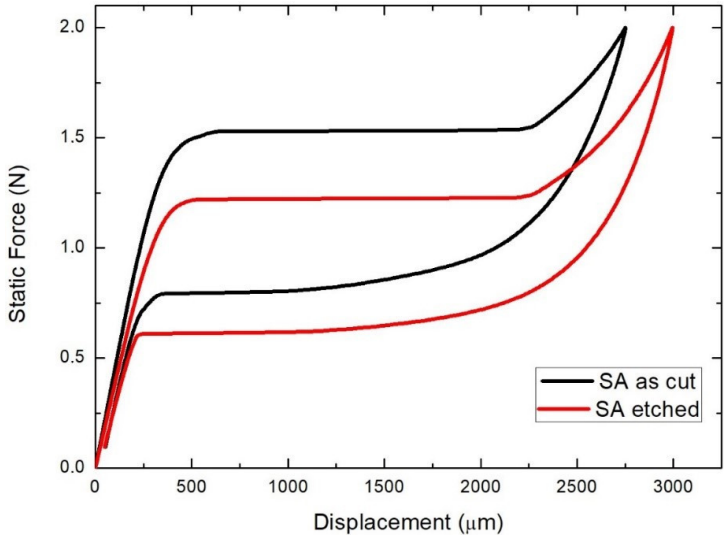

Figure 10. Comparison of static force/displacement curves at 30 °C before and after chemical etching.

The DSC scans of the laser-cut sample were analysed and compared with those of the initial material present in the CW condition (see Figure 11). Nno evident peaks of the martensitic transformation could be observed in the initial CW material; similarly, after laser cutting, the DSC scan exhibited some peaks upon heating and cooling. This may have been due to the effect of the laser cutting, which promoted the phase transformation. As in the case of the SA NiTi, no evident differences were seen in the DSC analysis. In the case of the CW NiTi, the material was overheated by the laser beam, and similar laser process conditions could provoke different responses in the material. The finer microstructure of the CW NiTi was more sensitive to the heat transfer, and this could induce a different thermal response of the material.

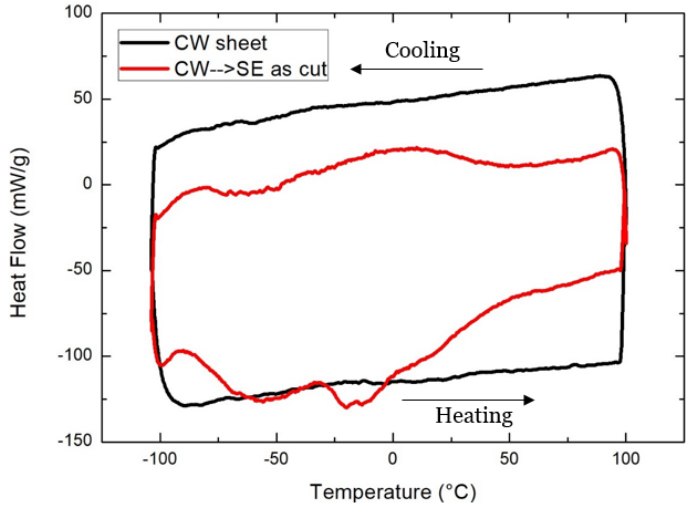

Figure 11. DSC curve of NiTi CW tape and NiTi diamond-like element in as-cut condition.

Figures 12 and 13 show the force–displacement curves of the CW diamond-like elements at varying testing temperatures and material conditions, respectively.

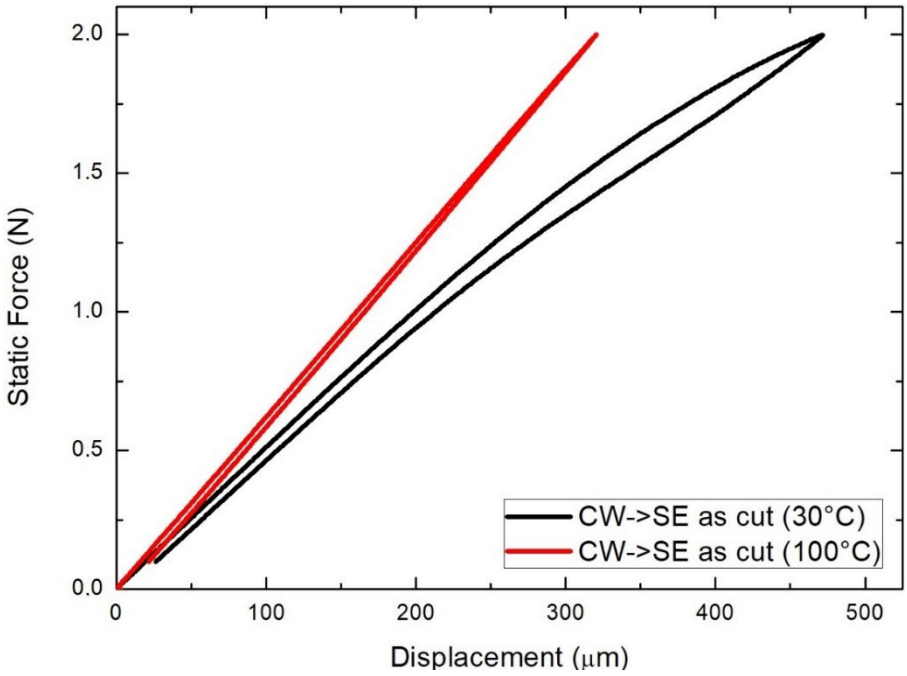

Figure 12. Static force/displacement curve for a diamond-like element cut from CW sheet at low (30 °C) and high (100 °C) temperatures.

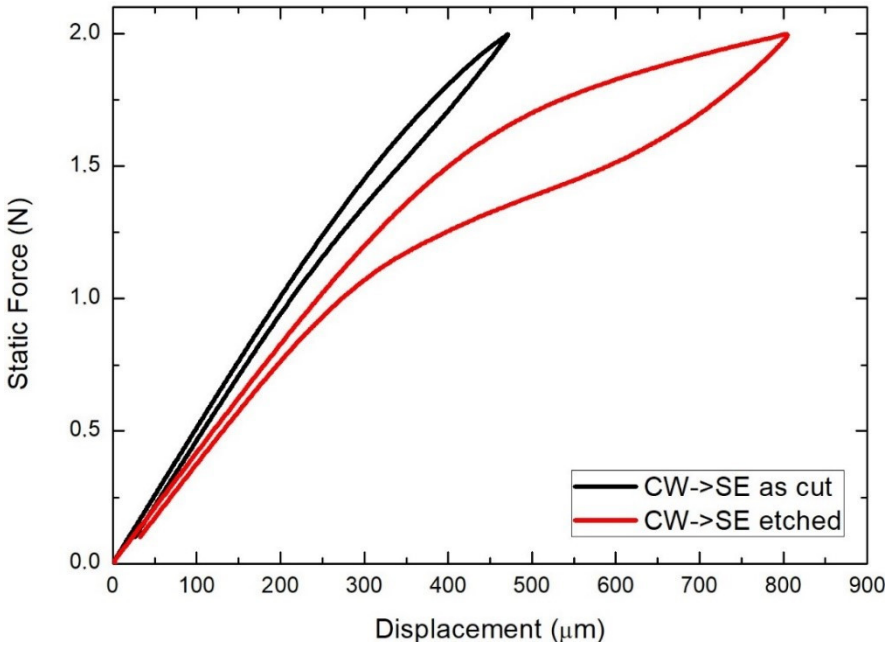

Figure 13. Static force/displacement curve for a diamond-like element cut from CW sheet before and after chemical etching.

The mechanical behaviour observed at 30 °C was not in a complete linear path, but a limited hysteretic loop was visible. The loading/unloading testing carried out at 100 °C highlighted a change in the Young modulus and maximal strain that occurred at the maximal force applied during the test. For better understanding the mechanical behaviour of the laser-cut element manufactured from the CW NiTi tape, Figure 13 shows the force–displacement curve of both the as-cut and etched samples. The chemical etching promoted

higher superelasticity, which allowed for reaching a maximal displacement of 800 μm, double than that of the case of the as-cut sample. This indicates that the chemical etching allowed for not only removing the thin layer of melted and overheated material, but also for highlighting that the NiTi element, previously in CW condition, was heat-treated with the laser processing to induce the martensitic transformation, as suggested in other papers in the literature [25,26].

The obtained superelastic response of the CW laser-cut diamond-like element could not be compared with the one from the SA element: the displacements were valued at 800 and 2800 μm, respectively. The transformation temperatures and the enthalpies of the martensitic transformation were also largely different for the CW laser-cut and SA elements. These differences can be explained by the fact that the CW material requires a more intense thermal cycle for promoting optimal functional performance, as expected from the SA material. Femtosecond laser cutting could also induce different thermal alterations, starting from different material conditions (CW vs. SA) that can be associated with different initial microstructures. The finer and stressed microstructure of the CW NiTi was more sensitive to the heat supplied by the laser beam than the SA sample was, which had previously been heat-treated. Consequently, some changes in material performance could be detected easier in the CW than those in the SA NiTi.

4. Conclusions

Optimal parameters for the femtosecond laser cutting of straight-annealed superelastic NiTi sheets were obtained and used as a starting point for the definition of the cutting of cold-worked sheets with the same laser. Straight-annealed diamond devices cut without any large thermal affection to the base material were used as a benchmark for superelasticity quality evaluation.

The process parameters adopted for cutting the cold-worked material generated superelasticity in the diamond-like elements through overheating imposed on the material during the machining. The higher thermal load given to the material was linked to the different properties of the cold-worked material compared to those of the straight-annealed one: the microstructure in first case was finer, and the sheet was not flat, causing problems of focusing that required 20% more scans to be used to cut through. The diamond-like elements manufactured from the cold-worked NiTi showed initial superelasticity that was largely minor with respect to the straight-annealed elements. This effect can be explained by the higher heat sensitivity of the cold-worked material, even to the limited heat transfer obtained in ultrashort laser processing. This study indicated that the plastic deformation degree and the next annealing for manufacturing NiTi components could be optimised in view of the laser cutting process.

Author Contributions: All authors have participated to all the activities regarding the preparation of the paper. All authors have read and agreed to the published version of the manuscript.

Funding: The authors would like to acknowledge Accordo Quadro CNR/Regione Lombardia n. 3866 FHfFC for their financial support.

Data Availability Statement: The data presented in this study are available on request from the corresponding authors.

Acknowledgments: The authors would like to thank Marco Bonfanti from Politecnico di Milano.

Conflicts of Interest: The authors declare no conflict of interest.

References

1. Otsuka, K.; Ren, X. Physical metallurgy of Ti–Ni-based shape memory alloys. *Prog. Mater. Sci.* **2005**, *50–55*, 511–678. [CrossRef]
2. Duerig, T.; Pelton, A.; Stoeckel, D. An overview of nitinol medical applications. *Mater. Sci. Eng. A* **1999**, *273–275*, 149–160. [CrossRef]
3. Jani, J.M.; Leary, M.; Subic, A.; Gibson, M.A. A review of shape memory alloy research, applications and opportunities. *Mater. Des.* **2014**, *56*, 1078–1113. [CrossRef]

4. Momma, C.; Knop, U.; Nolte, S. Laser cutting of slotted tube coronary stents—State of the art and future developments. *Prog. Mater. Res.* **1999**, *4*, 39–44.
5. Biffi, C.; Fiocchi, J.; Tuissi, A. Relevant aspects of laser cutting of NiTi shape memory alloys. *J. Mater. Res. Technol.* **2022**, *19*, 472–506. [CrossRef]
6. A Biffi, C.; Tuissi, A. Nitinol laser cutting: Microstructure and functional properties of femtosecond and continuous wave laser processing. *Smart Mater. Struct.* **2017**, *26*, 35006. [CrossRef]
7. Frenzel, J.; George, E.P.; Dlouhy, A.; Somsen, C.; Wagner, M.F.-X.; Eggeler, G. Influence of Ni on martensitic phase trans-formations in NiTi shape memory alloys. *Acta Mater.* **2010**, *58–59*, 3444–3458. [CrossRef]
8. Nespoli, A.; Biffi, C.A.; Previtali, B.; Villa, E.; Tuissi, A. Laser and Surface Processes of NiTi Shape Memory Elements for Micro-actuation. *Met. Mater. Trans. A* **2014**, *45*, 2242–2249. [CrossRef]
9. Biffi, C.A.; Bonacina, L.; Nespoli, A.; Previtali, B.; Tuissi, A. On the thermo-mechanical behavior of NiTi shape memory elements for potential smart micro-actuation applications. *J. Intell. Mater. Syst. Struct.* **2015**, *27*, 1875–1884. [CrossRef]
10. Biffi, C.A.; Bassani, P.; Carnevale, M.; Lecis, N.; Loconte, A.; Previtali, B.; Tuissi, A. Effect of laser microcutting on thermo-mechanical properties of NiTiCu shape memory alloy. *Met. Mater. Int.* **2014**, *20*, 83–92. [CrossRef]
11. Meijer, J. Laser beam machining (LBM), state of the art and new opportunities. *J. Mater. Process. Technol.* **2004**, *149*, 2–17. [CrossRef]
12. Phillips, K.C.; Gandhi, H.H.; Mazur, E.; Sundaram, S.K. Ultrafast laser processing of materials: A review. *Adv. Opt. Photon* **2015**, *7*, 684–712. [CrossRef]
13. He, Y.; Wang, L.; Wu, T.; Wu, Z.; Chen, Y.; Yin, K. Facile fabrication of hierarchical textures for substrate-independent and durable superhydrophobic surfaces. *Nanoscale* **2022**, *14*, 9392–9400. [CrossRef] [PubMed]
14. Li, G.; Nikumb, S.; Wong, F. An optimal process of femtosecond laser cutting of NiTi shape memory alloy for fabrication of miniature devices. *Opt. Lasers Eng.* **2006**, *44*, 1078. [CrossRef]
15. Stolberg, K.; Friedel, S.; Kremser, B.; Roehner, M. IR and green femtosecond laser machining of heat sensitive materials for medical devices at micrometer scale. *Proc. SPIE* **2014**, *8968*, 89680E.
16. Huang, H.; Zheng, H.; Lim, G. Femtosecond laser machining characteristics of Nitinol. *Appl. Surf. Sci.* **2004**, *228*, 201–206. [CrossRef]
17. Uppal, N.; Shiakolas, P.S. Micromachining Characteristics of NiTi Based Shape Memory Alloy Using Femtosecond Laser. *J. Manuf. Sci. Eng.* **2008**, *130*, 031117. [CrossRef]
18. Quintino, L.; Liu, L.; Miranda, R.M.; Silva, R.J.C.; Hu, A.; Zhou, Y. Cutting NiTi with Femtosecond Laser. *Adv. Mater. Sci. Eng.* **2013**, *2013*, 198434. [CrossRef]
19. Muhammad, N.; Li, L. Underwater femtosecond laser micromachining of thin nitinol tubes for medical coronary stent manufacture. *Appl. Phys. A* **2012**, *107*, 849–861. [CrossRef]
20. Levesque, T.; Perrottet, D.; Richerzhagen, B. Damage-free cutting of medical devices using the water-ject-guided laser. In Proceedings of the Materials and Processes for Medical Devices Conference, Boston, MA, USA, 14–16 November 2005.
21. Yung, K.C.; Zhu, H.H.; Yue, T.M. Theoretical and experimental study on the kerf profile of the laser micro-cutting NiTi shape memory alloy using 355 nm Nd:YAG. *Smart Mater. Struct.* **2005**, *14*, 337–342. [CrossRef]
22. Favier, D.; Liub, Y.; Orgéas, L.; Sandel, A.; Debovea, L.; Comte-Gaz, P. Influence of thermomechanical processing on the superelastic properties of a Ni-rich Nitinol shape memory alloy. *Mater. Sci. Eng. A* **2006**, *429*, 130–136. [CrossRef]
23. Li, Y.; Li, J.; Liu, M.; Ren, Y.; Chen, F.; Yao, G.; Mei, Q. Evolution of microstructure and property of NiTi alloy induced by cold rolling. *J. Alloys Compd.* **2015**, *653*, 156–161. [CrossRef]
24. Biffi, C.A.; Mathivanan, K.; Tuissi, A. Laser-Induced Superelasticity in NiTinol Stent Strut. *Shape Mem. Superelasticity* **2018**, *4*, 377–382. [CrossRef]
25. Tuissi, A.; Coduri, M.; Biffi, C.A. Laser shape setting of superelastic nitinol wires: Functional properties and microstructure. *Funct. Mater. Lett.* **2017**, *10*, 1740008. [CrossRef]
26. Biffi, C.A.; Tuissi, A. Laser shape setting of superelastic NiTi wire: Effects of laser beam power and axial pre-load. *Smart Mater. Struct.* **2019**, *28*, 075043. [CrossRef]